Numerical Modeling of the Mechanical Characteristics of the Magnetorheological Elastomers

Mateusz Kukla, *Krzysztof* Talaśka, *Aleksandra* Biszczanik, and *Jan* Górecki

Poznań University of Technology, Institute of Machine Design, 3 Piotrowo St., 60-965 Poznań, Poland

Abstract. The paper presents the work results associated with the implementation of the developed mathematical model describing the magnetorheological elastomers mechanical characteristics under compressive stress. The employed mathematical instrument constitutes the classic viscoelastic model development, accounting in its structure for the effect of the strain amplitude together with the magnetic field induction on the measured stress values progressive characteristic. The necessity to introduce such changes was demonstrated as a result of earlier studies. Within the this work scope, the structure of the developed numerical model is presented. Further provided are the results of carried out simulations, which are finally juxtaposed and compared with the earlier experiments results. This gives ground to evaluating the proposed model accuracy.

1 Introduction

The term ”Smart Materials” (adaptive materials, intelligent materials) is understood as a broad group of materials characterized by the change of their physical characteristics (e.g. viscosity) when exposed to another field (e.g. electromagnetic field) [1]. Their capabilities include, among others: detecting specific stimuli, processing the stimuli, typical reaction and return to initial state, all in the shortest possible time. The object of the current study are magnetorheological elastomers. These are classified as Smart Magnetic Materials (SMM). It is a relatively new material group undergoing dynamic development. Current studies by different centers focus on the manufacturing methods, material composition and structural formation of magnetorheological elastomers. Significant attention is directed to their practical applications. After year 2000 [1], there is an observed major increase in patent activity in regards to the material itself, but also its application. An analysis of solutions provided in subject literature allows to determine that the major area of use for magnetorheological elastomers focuses primarily on vibration dampers [2-5]. This application includes not only active control of linear vibration which use the discussed materials in compression [6] or shear [7, 8] modes of action, but also active control of torsional vibration [9, 10]. Many works were taken up involving the issue of mathematical representation of magnetorheological elastomers magnetic and mechanical characteristics. Despite this, no model to describe the behavior of magnetorheological elastomers was offered to date that would be deemed complete and finished. It is therefore justified to

continue the research effort in this regard. The present paper demonstrates the ongoing research results into the material characteristics and the possible application of magnetorheological elastomers in the broadly understood machine building [11, 2]..

2 Study methodology

2.1 Development of the mathematical model

As demonstrated earlier, the classic Kelvin-Voigt rheological model (viscoelastic material) cannot be deemed sufficient for the characteristics modeling of magnetorheological elastomers in a broad strain amplitude and excitation frequency range [11]. Considering the above, certain modifications were proposed to allow to account for the strain amplitude effect on the set of obtained results. One needs to emphasize that the variance of mechanical characteristics caused by excitation frequency, in the general case, cannot be omitted. The problems associated with the examination of this dependence are the subject matter of planned further studies. The developed mathematical model can be expressed as follows [11]:

$$\sigma(t) = E_{mod}\varepsilon(t) + \eta\dot{\varepsilon}(t), \tag{1}$$

where: $\sigma(t)$the time course of a stress function, $\varepsilon(t)$the time course of a strain function, $\dot{\varepsilon}(t)$ stands for strain rate, E_{mod} is the modified stiffness coefficient, η represents the coefficient of viscosity. Considering that excitation shall be a known sinusoidal waveform of strain with respect to time, the formula (1) can be expressed as:

$$\sigma(t) = \frac{pE}{1 - q\varepsilon_0 \sin(\omega t)} \cdot \varepsilon_0 \sin(\omega t) + \eta\omega \cdot \varepsilon_0 \cos(\omega t), \tag{2}$$

where: p and q are the parameters for the hysteresis loop shape, whereas E stands for the stiffness coefficient (classic model for viscoelastic body). The respective values in model (2) can be also characterized with the following dependence (3):

$$E' = E \text{ and } E'' = \eta\omega, \tag{3}$$

where E' stands for storage modulus, whereas E'' represents the loss modulus.
In the presented model, the viscosity coefficient η is a linear function of magnetic field induction B. The modified stiffness coefficient E_{mod} is the function of strain, the hysteresis loop shape parameters p and q as well as the magnetic field induction B (indirectly via the stiffness coefficient E).
So as to increase the representation accuracy of actual results, it was decided to utilize a higher number of hysteresis loop shape parameters than two (p and q). The results analysis of tests carried out to date [12-14] allows to determine that the highest variance in the registered hysteresis loops characterizes the material loading (upper part of the hysteresis loop) from the half of the value of strain amplitude. As regards the lower part of the characteristic, being responsible for unloading, one observes similar behavior of the graph lines; however they are occurring for different strain values. It was determined that the range in which the variety of the characteristic is the highest occurs from the maximum strain value ε_0 up to the value equal to $0.69\varepsilon_0$. It was therefore decided that this value shall constitute the threshold in the variability range of hysteresis loop shape parameters. On this basis, eight parameters of hysteresis loop shape were selected ($p_{11,12}$, $p_{21,22}$ oraz $q_{11,12}$, $q_{21,22}$). A schematic representation of the graphical interpretation and hysteresis loop shape

parameters assumption method is provided on Fig. 1. As a consequence of assuming a higher number of parameters, the expression (2) was modified with the resultant expression being (4):

$$\sigma(t) = \begin{cases} \dfrac{p_{11}(B)}{1 - q_{11}(B)\varepsilon_0 \sin(\omega t)} \cdot E(B)\varepsilon_0 \sin(\omega t) + (\eta\omega)(B)\varepsilon_0 \cos(\omega t) & \text{for } \dot{\varepsilon} \geq \text{ and } \varepsilon \leq 0.5\varepsilon_0, \\ \dfrac{p_{12}(B)}{1 - q_{12}(B)\varepsilon_0 \sin(\omega t)} \cdot E(B)\varepsilon_0 \sin(\omega t) + (\eta\omega)(B)\varepsilon_0 \cos(\omega t) & \text{for } \dot{\varepsilon} \geq \text{ and } \varepsilon > 0.5\varepsilon_0, \\ \dfrac{p_{21}(B)}{1 - q_{21}(B)\varepsilon_0 \sin(\omega t)} \cdot E(B)\varepsilon_0 \sin(\omega t) + (\eta\omega)(B)\varepsilon_0 \cos(\omega t) & \text{for } \dot{\varepsilon} < \text{ and } \varepsilon \leq 0.69\varepsilon_0, \\ \dfrac{p_{22}(B)}{1 - q_{22}(B)\varepsilon_0 \sin(\omega t)} \cdot E(B)\varepsilon_0 \sin(\omega t) + (\eta\omega)(B)\varepsilon_0 \cos(\omega t) & \text{for } \dot{\varepsilon} < \text{ and } \varepsilon > 0.69\varepsilon_0. \end{cases} \quad (4)$$

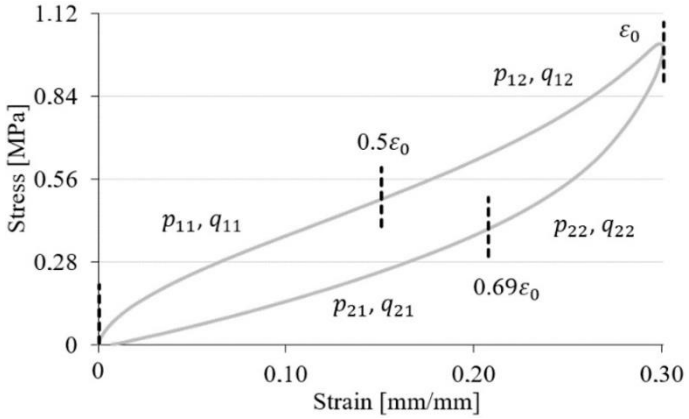

Fig. 1. Graphic interpretation and assumption method of hysteresis loop shape parameters.

2.2 Determination of model parameter values

Numerical values determination for the modified Kelvin-Voigt model parameters required carrying out a number of calculations. To this end, the authors proposed an algorithm of their own development allowing to calculate the values of parameters q and p as a magnetic field function, based on earlier measurements, as discussed in [12, 13]. The diagram for hysteresis loop shape parameters determination is provided on Fig. 2 below.

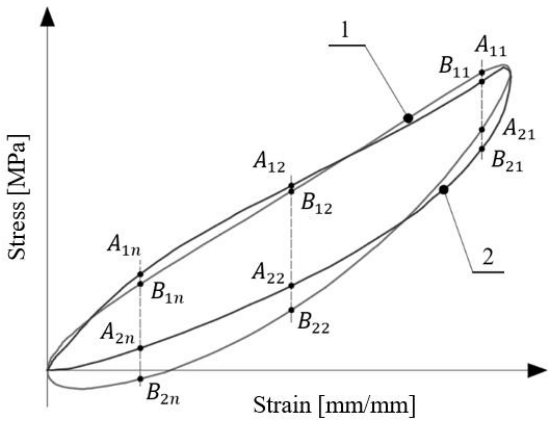

Fig. 2. Diagram for hysteresis loop shape parameters p and q determination; 1 – the hysteresis loop determined on the basis of the modified Kelvin-Voigt model, 2 – the hysteresis loop achieved from measurement results.

The method to determine the parameters p and q values is based on such their values selection that the sum of squares of differences between the loops obtained on as a result of modeling and from measurements is as small as possible. In the first stage of calculation the two hysteresis loops are determined. Next, the table of p and q values is developed with significant dispersion. In order to achieve the best possible actual characteristics representation, two parameters pairs are determined separately for the upper part of the hysteresis loop $p_{11,12}$ and $q_{11,12}$, as well as separately for the bottom part $p_{21,22}$ and $q_{21,22}$. Through these determined curves, n lines parallel to the ordinate (stress axis) are drawn. In this way, the algorithm defines the set of points A_{11}, … , A_{1n}, and B_{11}, … , B_{1n}, (for the upper part of the loop) and A_{21}, … , A_{2n}, as well as B_{21}, … , B_{2n}, (for the bottom part of the loop), as shown on Fig 2. Thus, the lengths of sections are determined $|A_{11}B_{11}|$, …, $|A_{1n}B_{1n}|$ and $|A_{21}B_{21}|$, …, $|A_{2n}B_{2n}|$. These values result from the discrepancy between the actual hysteresis loop and the loop achieved from the model. This constitutes the measurement of model's inaccuracy. Afterwards, the sums of squares of section lengths determined in the previous step are determined. These are defined as $l_1 = \sum(|A_{11}B_{11}|^2 + \ldots + |A_{1n}B_{1n}|^2)$ for the upper part of the loop and $l_2 = \sum(|A_{21}B_{21}|^2 + \ldots + |A_{2n}B_{2n}|^2)$ for the bottom part of the hysteresis loop. The algorithm searches the resultant values set l_1 and l_2 for all the assumed p and q values and selects the variant for which these values are the lowest (i.e. the following conditions are met: $l_1 \rightarrow min$ and$l_2 \rightarrow min$). In the following stage, the parameter values for p and q are re-assumed with low scatter, close to the values which were defined in the previous step. This process aims to determine the sought parameters exact value. Afterwards, the data set for l_1 and l_2, is determined once again and the algorithm searches for the lowest values to indicate the final values for $p_{11,12}$, $p_{21,22}$ and $q_{11,12}$, $q_{21,22}$.

In the earlier studies [12, 13], the stress-strain curves (hysteresis loops) for magnetorheological elastomer samples were registered at different strain amplitude $\varepsilon_0$values and magnetic induction B. These were used as a basis for the parameters determination for the described mathematical model. First of all, the averaged moduli values were determined: the storage modulus E' and loss modulus E'' in the Kelvin-Voigt model (Fig. 3). Finally, the values for the hysteresis loop shape parameters $p_{11,12}$, $p_{21,22}$ and $q_{11,12}$, $q_{21,22}$ were determinedin accordance to the presented methodology (Fig. 4 and 5).

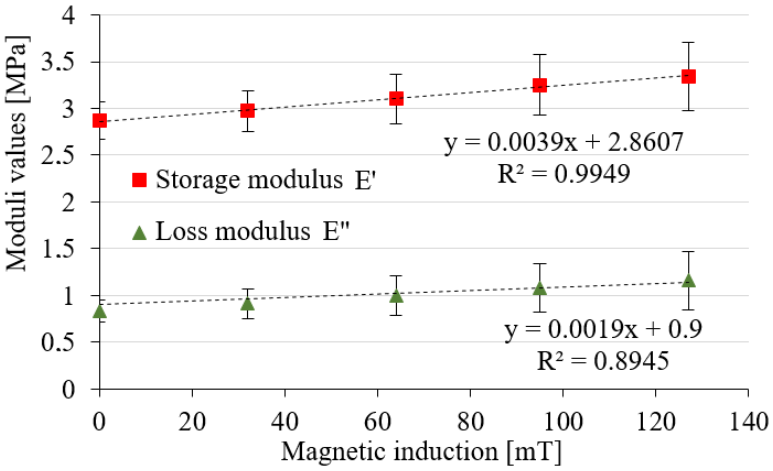

Fig. 3. Averaged values for the storage modulus *E'* and loss modulus *E"* as a function of magnetic induction assumed for the modified Kelvin-Voigt model.

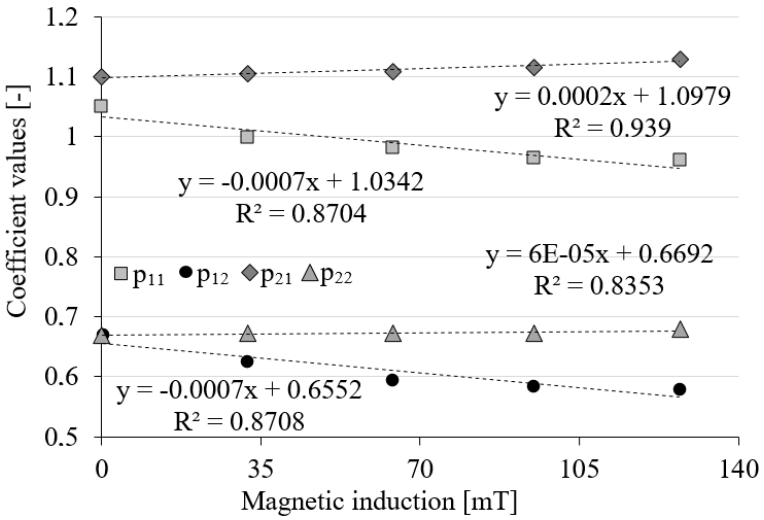

Fig. 4. Determined coefficient values p_{11}, p_{12}, p_{21}, p_{22} as a function of magnetic induction B.

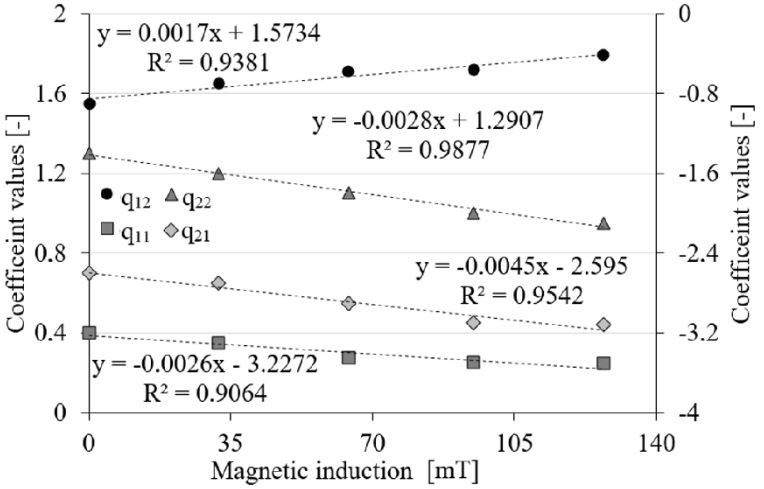

Fig. 5. Determined coefficient values q_{11}, q_{12}, q_{21}, q_{22} as a function of magnetic induction B.

Presented graphs analysis indicates variance of the model parameters caused by the magnetic field. The determined values of parameters p_{11}, p_{12}, p_{21}, p_{22} exhibit a good match to a linear function. Coefficient of determination R^2 values, being close to one, indicate the very high representation accuracy of parameters q_{11}, q_{12}, q_{21}, q_{22}value variance by employing a linear function. What follows from the presented data, the highest degree of accuracy in hysteresis loop representation in the developed model calls for assuming negative values of parameters q_{11} and q_{21}.

2.3 Model implementation in the environment for numerical calculations

MATLab Simulink software package components were usedin the development of the model as defined in the previous chapter. The software enables carrying out simulations and calculations in real time. The implemented model view in this environment as well as its structure comprising three components defining the characteristics of the examined composite as appropriate, are provided in the schematic view on Fig. 6. The model component marked with 1 is responsible for modeling the viscous characteristics. These are dependent on the loss modulus$E$'', which is described by the expression (3). This function is a linear dependence of the magnetic field induction B, in accordance with the dependencies provided on Fig.3. The subsequent model's components, marked with numbers from 2 to 5, determine: the upper and lower part of the hysteresis loop. At the same time, functions for the storage modulus E' and hysteresis loop shape parameters $p_{11,12}$, $p_{21,22}$ and $q_{11,12}$, $q_{21,22}$ are used, with linear dependence on the magnetic field induction B, in accordance with the dependencies provided on Fig. 4 and 5.

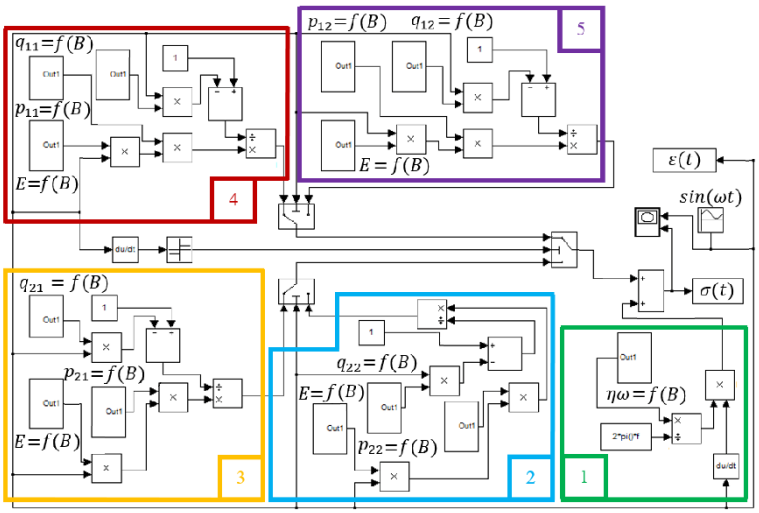

Fig. 6. View of the mathematic model implemented in the environment for numerical calculations MATLab Simulink; 1 – system component modeling viscous characteristics (representing the loss modulus *E''*), 2 – system component modeling the elastic characteristics for the second's part lower section of the hysteresis loop, 3 – system component modeling the elastic characteristics for the first part's lower section of the hysteresis loop, 4 – system component modeling the elastic characteristics for the upper section's first part of the hysteresis loop, 5 – system component modeling the elastic characteristics for the upper section's second part of the hysteresis loop.

3 Study results and analysis

3.1 Results of numerical calculations

Fig. 7 presents the selected characteristics determined on the basis of numerical calculations results obtained from the developed model. The presented graphs analysis indicates variance in the obtained results resulting from the substitution of different magnetic induction *B* values. Further visible is the increasing progression of the characteristics following the strain value increase. It is also possible to observe the variance in progression degree for the earlier defined strain value ranges which is reflected in the change in individual section of the hysteresis loop slope angle. This serves to prove that the goal of the modification introduced into the material model was achieved. A comparison of example hysteresis loops determined in the course of study and the results obtained from simulations using the developed numerical model are provided below on Fig. 8.

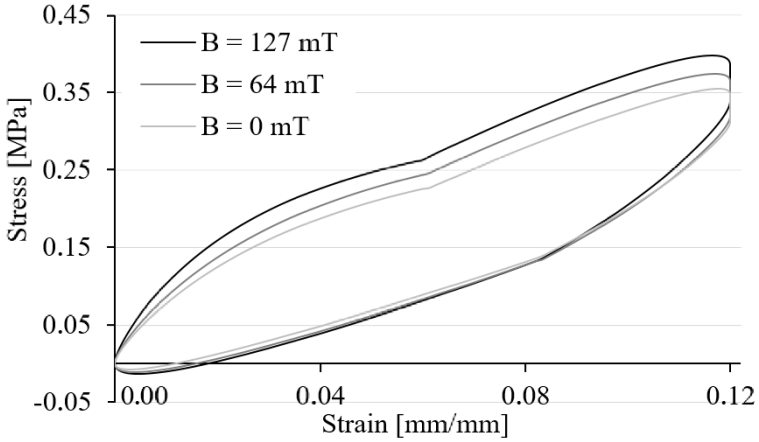

Fig. 7. Juxtaposition of hysteresis loops as a function of magnetic induction B determined using the numerical model for frequency f = 0.47 Hz and strain amplitude ε= 12%.

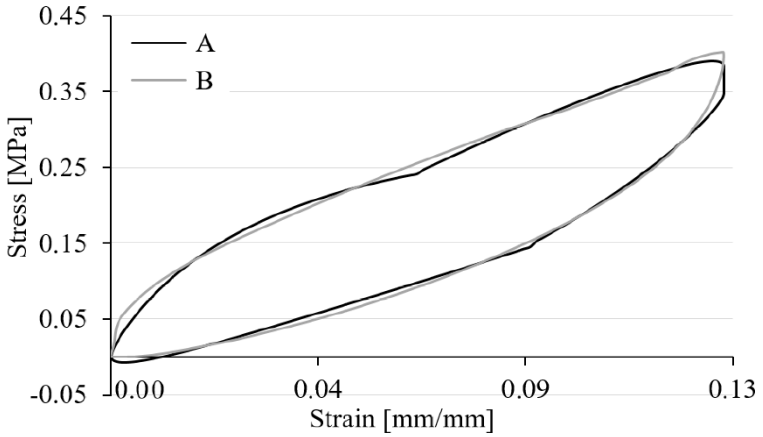

Fig. 8. Juxtaposition of hysteresis loops: A – from numerical model for frequency f = 1.35 Hz, strain amplitude ε= 13% and magnetic field induction B= 0 mT, B – determined in actual test.

An analysis of the provided graphs shows that the biggest errors in stress value determination appear in the extreme strain values vicinity. A quality evaluation of the modified numerical model was therefore attempted. In order to determine the error value, it is necessary to utilize the measured stress value in a given time limit $\sigma_{rz}(t_n)$, as well as the stress value in a given time limit from the model $\sigma_{num}(t_n)$. The deviation of the modified numerical model in the given time limit is defined as below (5):

$$\Delta\sigma(t_n) = \left|\frac{\sigma_{rz}(t_n) - \sigma_{num}(t_n)}{\sigma_{rz}(t_n)}\right| \cdot 100\%. \quad (5)$$

The numerical model allows to set any time of progression, allowing to determine the stress value at any time limit t_n. This was used to determine the error value as a function of time for individual points of measurement in the entire strain range. The scheme representing the

error value determination of the numerical model $\Delta\sigma(t_n)$ is provided on Fig. 9. The selected determination results of the model error value are provided on Fig. 10.

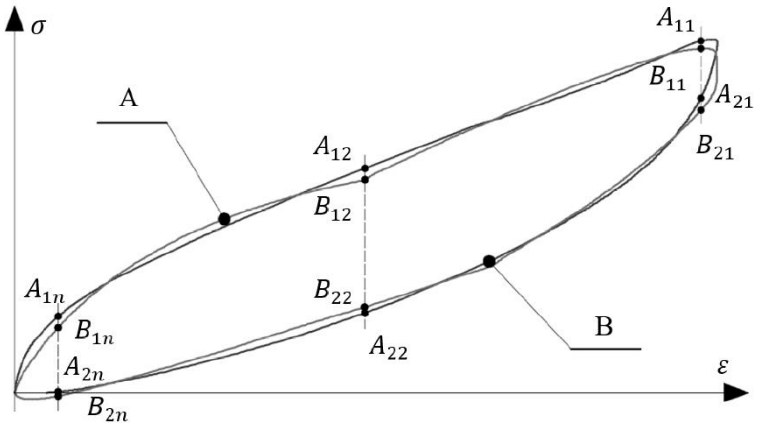

Fig. 9. The scheme of determining the numerical model error value $\Delta\sigma(t_n)$; A – the hysteresis loop determined through modeling, B – the hysteresis loop registered during the study.

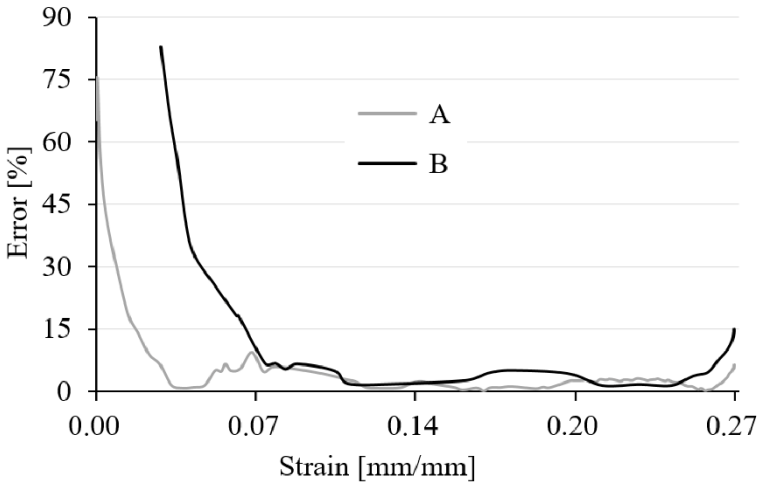

Fig. 10. Error value $\Delta\sigma(t_n)$ of the developed numerical model for frequency f = 1.55 Hz, strain amplitude ε = 27% and magnetic field induction B = 127 mT; A – loading, B – unloading.

As follows from the analysis of the presented graphs, the agreement between the numerical model and the measured data is unsatisfactory for very low strain values. This stems in part from the assumptions regarding the linear influence of the magnetic induction on the model parameters, and in part from the imperfections in the Kelvin-Voigt model. The result of modifications introduced to the model (implemented hysteresis loop shape parameters: p_{11}, p_{12}, p_{21}, p_{22} oraz q_{11}, q_{12}, q_{21}, q_{22}) brings about an improved consistency between the results of numerical analysis and actual measured results for higher strain values. The range and character of changes observed in the characteristics received from the numerical model are satisfactory in comparison to the observed behavior of the magnetorheological elastomer in the course of the experimental study. It should be pointed out that in a certain

selected range (excluding low strain values), the deviation of the proposed model oscillates in a satisfactory error raterange. This is shown on Fig. 11 and 12.

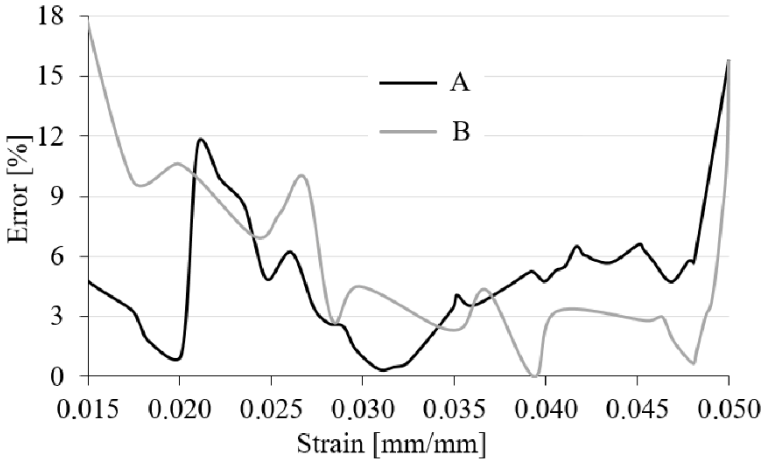

Fig. 11. Error rate $\Delta\sigma(t_n)$ for the developed numerical model, excluding low strain values for frequency f= 0.55 Hz, strain amplitude ε = 5% and magnetic field induction B= 64 mT; A – loading, B – unloading.

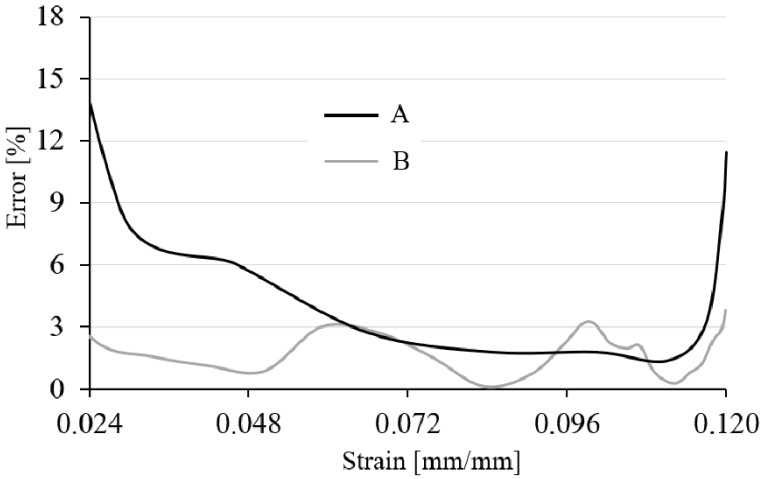

Fig. 12. Error rate $\Delta\sigma(t_n)$ for the developed numerical model, excluding low strain values for frequency f = 0.47 Hz, strain amplitude ε = 12% and magnetic field induction B = 0 mT; A – loading, B – unloading.

4 Summary

A detailed variance analysis shown by the characteristics obtained in actual measurements and characteristics obtained in numerical calculations allow to ascertain that the model offers an adequate representation of actual values only above a specific value of strain amplitude. Higher discrepancy is observed, the more the strain value in the given time limit differs from its maximum value. The assumed model allows to describe the loop in the

shape of an ellipsis. Therefore, certain differences between hysteresis loops determined numerically and actual hysteresis loops cannot be avoided. It should be concluded that the influence of the increasing cross-section of the examined samples is highly important. The variance range in characteristics of magnetorheological elastomer resulting from this phenomenon exceeds the variance range effected by the magnetic field. This is highly disadvantageous as the effects of these phenomena tend to overlap, increasing the difficulty of mathematical modeling. Taking into consideration the strain amplitude and frequency of excitation in a broader range than was proposed calls for performing additional studies focusing on the exact determination of the character of changes occurring as a result of significant crosswise strain (change in the cross-section of the examined samples of magnetorheological elastomers).

References

1. J. Kaleta Magnetic materials SMART. Construction, production, properties testing, application. Publishing House of the Wrocław University of Technology (2013).
2. A. K. Bastola, M Paudel, L. Lin 3D Printed Magnetorheological Elastomers. Proc. of the ASME Conf. on Smart Mat. Adaptive Str. and Int. Sys. (Snowbird) vol 1**,** SMASIS 2017-3732 1-5 (2017).
3. H.M.N. Hadzir, Z.A. Norfaidayu, M.S.M. Sabri, M.-H. Abu-Bakar Investigation of damping coefficient for magnetorheological elastomer. MATEC Web of Conf., 217, 02003-1-7 (2018).
4. V. Kumar, D.-J. Lee Iron particle and anisotropic effects on mechanical properties of magneto-sensitive elastomers 2017 J. of Mag. and Mag. Mat., 41, 105-12 (2017).
5. J.Y. Lee, V. Kumar, D.J. Lee Compressive properties of magnetorheological elastomer with different magnetic fields and types of filler. Pol. for Adv. Techn, .30, 1106-15 (2019).
6. S.S. Sun, Y. Chen, J. Yang, T.F. Tian, H.X. Deng, W.H. Li, H. Du, G. Alici The development of an adaptive tuned magnetorheological elastomer absorber working in squeeze mode. Smart Mat. and Str,.23, 1-8 (2014).
7. H. Deng, X. Gong Application of magnetorheological elastomer to vibration absorber Comm. in Nonlinear Sci. and Numerical Sim., 13, 1938-47 (2008)
8. G.J. Liao, X.L. Gong, C.J. Kang, S.H. Xuan The design of an active-adaptive tuned vibration absorber based on magnetorheological elastomer and its vibration attenuation performance. Smart Mat. and Str., 20, 1-10 (2011).
9. N. Hoang, N. Zhang, H. Du An adaptive tunable vibration absorber using a new magnetorheological elastomer for vehicular powertrain transient vibration reduction. Smart Mat. and Str.**,** 24, 2036-44 (2010).
10. T. Mitsumata, S. Ohori Magnetic Polyurethane Elastomers With Wide Range Modulation of Elasticity. Pol. Chem., 2, 1063-67 (2011).
11. M. Kukla Modeling selected mechanical properties of magnetorheological elastomers, IOP Conf. Series: Mat. Sci. and Eng., 776, 012079, 1-7 (2020).
12. M. Kukla, A. Fierek, M. Berdychowski, M. Kończak The study of mechanical properties of magnetorheological elastomers under compressive stress. IOP Conf. Series: Mat. Sci. and Eng.*,* 776**,** 012079, 1-8 (2020).

13. M. Kukla, J. Górecki, I. Malujda, K. Talaśka, P. Tarkowski The Determination of Mechanical Properties of Magnetorheological Elastomers (MREs). Procedia Eng., 177, 324-30 (2017).
14. M. Kukla Shaping the material properties of magnetorheological elastomers in mechanical engineering. *Doctor's thesis*, Poznań: Poznan University of Technology (2018).